Predictability and Genesis of Hurricane Karl (2010) Examined through the EnKF Assimilation of Field Observations Collected during PREDICT

JONATHAN POTERJOY AND FUQING ZHANG

Department of Meteorology, The Pennsylvania State University, University Park, Pennsylvania

(Manuscript received 12 September 2013, in final form 26 November 2013)

ABSTRACT

The genesis of Hurricane Karl (2010) is explored using analyses and forecasts from a cycling ensemble Kalman filter (EnKF) that assimilates routinely collected observations as well as dropsonde measurements that were taken during the Pre-Depression Investigation of Cloud Systems in the Tropics (PREDICT) field campaign. A total of 127 dropsonde observations were collected from six PREDICT flight missions over a 5-day period before and during Karl's genesis. EnKF analyses that take into account the PREDICT dropsondes provide a detailed four-dimensional overview of the evolving kinematic and thermodynamic structure within the pregenesis disturbance. In particular, the additional field observations are found to increase the low- and midlevel circulation and column moisture in the EnKF analyses and reduce the position error of the low-level vortex. Deterministic forecasts from these analyses show a 24-h improvement in predicting genesis over a control experiment that omits the dropsonde observations. In ensemble forecasts for this event, the more accurate analyses translate into a higher confidence in predicting the intensification of Karl; that is, data assimilation experiments also suggest that initial condition errors at the mesoscale pose large challenges for predicting genesis, thus highlighting the need for improved observation networks and more advanced data assimilation methods.

1. Introduction

The formation of a tropical cyclone is typically preceded by the development of a synoptic-scale disturbance—for example, a low pressure system along a tropical wave, a monsoon trough, or an extratropical cyclone. For the case of tropical waves, observational and modeling studies support a range of explanations as to how a tropical weather system can generate a self-sustained cyclone. Among these studies, some propose a "top down" process in which stratiform precipitation associated with mesoscale convective systems within the synoptic-scale disturbance acts to moisten and cool the column of air between the lower and middle troposphere, which leads to a gradual lowering of the midlevel cyclone (Bister and Emanuel 1997; Ritchie and Holland 1997; Simpson et al. 1997). An alternative theory suggests that genesis follows a "bottom up" process, in which the low-level cyclonic circulation intensifies via the merging of convectively induced vorticity anomalies (Hendricks et al. 2004; Reasor et al. 2005; Montgomery et al. 2006; Halverson et al. 2007). More recent studies emphasize a multiscale pathway to genesis. Dunkerton et al. (2009) hypothesize that genesis is favored within a region of approximately closed Lagrangian circulation in the synoptic-scale disturbance, where cloud-scale vorticity anomalies are protected from the entrainment of relatively dry environmental air. Vorticity and column moisture are allowed to build up in this region until the eventual formation of a tropical cyclone. Fang and Zhang (2010, 2011) show that accumulative heating from convective cells within the vortex can amplify the quasi-balanced system-scale circulation, which in turn produces a secondary circulation that organizes the cloud-scale vorticity anomalies.

Regardless of the path to genesis, the process by which a tropical cyclone forms and intensifies is sensitive to the synoptic- and mesoscale wind and moisture features in the pregenesis disturbance. In ensemble simulations of developing and nondeveloping tropical cyclones, Sippel and Zhang (2008, 2010) found genesis and intensification to be highly sensitive to the amount of deep moisture and convective available potential energy (CAPE) in the initial conditions. Zhang and Tao (2013) showed that

Corresponding author address: Professor Fuqing Zhang, Department of Meteorology, The Pennsylvania State University, 503 Walker Building, University Park, PA 16801.
E-mail: fzhang@psu.edu

DOI: 10.1175/JAS-D-13-0291.1

vertical wind shear further decreases the predictability of intensity by amplifying the effects of small-scale errors in the moisture field. They found that differences in moist convection could alter the tilt amplitude and angle of the incipient tropical storm vortex, which can lead to significant differences in the onset of genesis and rapid intensification. Using empirical orthogonal functions (EOFs), Torn and Cook (2013) found ensemble forecasts for the genesis of Hurricanes Danielle and Karl (2010) to be most sensitive to the low-level circulation and the mid- to upper-level thermodynamic fields of the pregenesis system, with a smaller sensitivity to the environmental conditions. From these studies, it follows that the skill of a numerical model in predicting genesis must depend on the availability of observations and the effectiveness of a data assimilation system in generating accurate initial conditions.

The Pre-Depression Investigation of Cloud Systems in the Tropics (PREDICT) field campaign was carried out during the 2010 Atlantic hurricane season to collect detailed dropsonde observations in the vicinity of tropical waves prior to the development of a tropical depression (Montgomery et al. 2012). With the ultimate goal of finding new precursors for genesis, the targeted tropical waves include weather systems that formed and did not form tropical cyclones. One objective of the PREDICT experiment is to examine the predictability of tropical cyclogenesis with state-of-the-art ensemble analysis and forecasting systems. Two experimental ensemble Kalman filter (EnKF) data assimilation systems based on the Weather Research and Forecast model (WRF) were used during PREDICT to provide short-range (24–72 h) guidance for mission planning. Examples of real-time ensemble forecasts from these two systems are presented in Montgomery et al. (2012). Given the initial condition and modeling uncertainty associated with tropical cyclogenesis forecasts, this aspect of the experiment requires high-resolution in situ observations to explore both the practical and intrinsic predictability of genesis.

To investigate the potential benefits of assimilating field observations near a pregenesis tropical disturbance, the current study uses an ensemble data assimilation system that was used in real time for PREDICT (i.e., The Pennsylvania State University WRF-EnKF). All conventional nonradiance data along with dropsondes collected during PREDICT flight missions are assimilated over a 10-day period in which a tropical disturbance transitioned into Hurricane Karl (2010). Analyses from three sets of cycling data assimilation experiments are compared to explore the synoptic- and mesoscale evolution of the tropical weather system prior to genesis. The first two experiments use a 13.5-km domain to examine the utility of PREDICT observations in producing accurate analyses of Karl, while the third experiment uses a 4.5-km domain to test the sensitivity of the data assimilation to model resolution. Both deterministic and ensemble forecasts are used to assess changes in predictability for Karl at different lead times during the cycling.

The organization of the manuscript is as follows. Section 2 provides a synopsis of Hurricane Karl and presents the timeline for the PREDICT flight missions leading up to genesis. It also describes the model and data assimilation systems used during this study as well as the design of the cycling data assimilation experiments. Section 3 contains an overview of the analysis results from the set of data assimilation experiments, while sections 4 and 5 present deterministic and ensemble forecast results, respectively. Section 6 compares results from the 13.5- and 4.5-km data assimilation experiments and section 7 summarizes the conclusions of this study.

2. Experiment setup

a. Overview of Hurricane Karl and the PREDICT dropsondes

Karl was a major hurricane from the 2010 Atlantic season that formed in the northwestern Caribbean Sea and made landfall twice on the coast of Mexico. It developed from a broad westward-propagating cyclone that initiated near the northern coast of South America on 8 September. The National Hurricane Center (NHC) began forecasting a medium to high 48-h probability of genesis as early as 9 September, but the actual depression did not form until 1200 UTC 14 September (Stewart 2010). Owing to its slow development, the pre-Karl disturbance was the most observed event during the PREDICT field campaign. In the 5 days leading up to genesis, six flight missions were carried out using the National Science Foundation (NSF)–National Center for Atmospheric Research (NCAR) Gulfstream V (GV) aircraft (Montgomery et al. 2012). Shortly after becoming a named tropical storm, Karl passed over the Yucatan Peninsula and rapidly intensified into a strong Category 3 hurricane on the Saffir–Simpson scale. Predicting the intensity of Karl remained a great challenge for forecasters, even after it became a self-sustained tropical cyclone. Karl's rapid intensification over the Bay of Campeche was not represented well in operational forecast models, which led to official intensity forecast errors that were well above average (Stewart 2010). Figure 1 summarizes the track and intensity changes of the weather system, starting from the pre-Karl disturbance

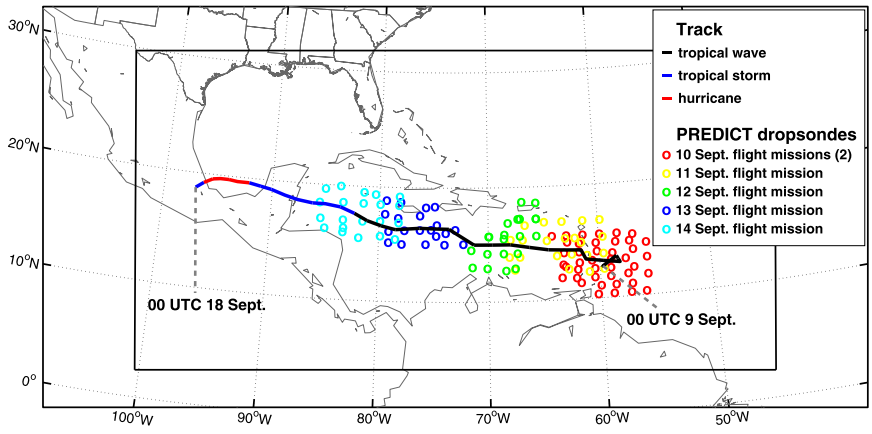

FIG. 1. The location of the tropical weather system is indicated prior to genesis (black), during tropical storm intensity (blue), and during hurricane intensity (red). Dropsonde locations are indicated by the circles on 10 (red), 11 (yellow), 12 (green), 13 (dark blue), and 14 Sep (light blue).

on 9 September and ending with its decay over Mexico on 18 September. Intensity and track observations of the tropical cyclone are taken from the NHC best-track dataset, while the pregenesis storm positions come from the wave tracking product described in Wang et al. (2012). The figure also indicates the positions of PREDICT dropsonde observations that were collected during each flight mission. These dropsondes were launched at altitudes between 150 and 200 hPa, and span a region that covers the inner 7.5° (~800 km) of the storm center.

b. WRF

The Advanced Research WRF version 3.4.1 (Skamarock et al. 2008) is used for this study with an outer domain that covers the Gulf of Mexico and Caribbean Sea with a 251 × 226 horizontal grid at a spacing of 13.5 km (black box in Fig. 1). A two-way nested inner domain follows the disturbance using a 253 × 253 horizontal grid at a spacing of 4.5 km. Each domain has 35 vertical levels, most of which are concentrated in the lower troposphere, and a model top of 5 hPa. The physical parameterization schemes include WRF single-moment 6-class microphysics (Hong et al. 2004), the Rapid Radiative Transfer Model (RRTM) (Mlawer et al. 1997) and Dudhia (Dudhia 1989) radiation schemes, Monin–Obukhov similarity (Monin and Obukhov 1954) for the surface layer, five-layer thermal diffusion for surface layer physics, and the Yonsei University planetary boundary layer scheme (Noh et al. 2003). Sensitivity experiments with and without the parameterization of cumulus physics show improved results when convection was represented explicitly in both domains, so cumulus parameterization is turned off for this case study.

c. WRF-EnKF data assimilation

This study uses the WRF-EnKF data assimilation system developed originally by Meng and Zhang (2008a,b), and adapted later for tropical cyclones in Zhang et al. (2009, 2011) and Weng and Zhang (2012). Since 2008, this system has been used in real time to assimilate routinely collected radial velocity observations from NOAA P3 airborne Doppler radar flight missions and provide forecasts for tropical cyclones in the Atlantic hurricane basin. The EnKF uses an ensemble forecast to advance a flow-dependent background error covariance matrix between data assimilation cycles, thus acting as an approximation to the extended Kalman filter (Evensen 1994). Ensemble perturbations are updated around the posterior mean state using the square root algorithm described in Whitaker and Hamill (2002). To treat sampling errors, the ensemble-estimated background covariance is localized using an element-wise multiplication of the covariance matrix with a Gaspari and Cohn (1999) fifth-order correlation function, and perturbations are inflated after each analysis using the "covariance relaxation to the prior" method proposed in Zhang et al. (2004). For this study, the EnKF uses 60 members with a horizontal localization radius of 900 km, a vertical localization radius of 15 vertical levels, and a relaxation coefficient of 0.8 (i.e., 80% of the updated perturbation is relaxed back to the prior). See Poterjoy et al. (2014) for a discussion on sampling errors pertaining to this data assimilation system.

d. Experiment design

Perturbations are sampled from a climatological background error covariance matrix[1] and added to the Global Data Assimilation System (GDAS) analysis at 1800 UTC 7 September to generate the initial ensemble of model states. The ensemble members are then integrated forward for 12 h before assimilating the first set of observations at 0600 UTC 8 September. This integration period enables the ensemble to develop physically consistent flow-dependent covariance structures before the first cycle. The GDAS data are also used throughout the experiments to provide lateral boundary conditions for the limited-area model, and to provide sea surface temperatures that remain fixed throughout each simulation.

Following the first ensemble forecast, the EnKF assimilates all nonradiance observations from the NOAA Meteorological Assimilation Data Ingest System (MADIS) every 6 h between 0600 UTC 8 September and 0000 UTC 18 September. These observations include surface data, routine soundings, and cloud-tracked winds from Geostationary Operational Environmental Satellites (GOES). Observations that are collected within 3 h of the analysis time are assimilated at a given cycle using the same time stamp as the analysis. The beginning of the cycling period corresponds to the first identification of the pre-Karl disturbance by the NHC, and the last cycle occurs as Karl decays over the Mexican coast. This data assimilation experiment (denoted "EnKF-MADIS") provides the control in our study, since field observations are not used in the analyses. In a second experiment (denoted "EnKF-PREDICT") the data assimilation is repeated from 1200 UTC 10 September to the end of the cycling period to generate a set of analyses that takes into account both the MADIS and the PREDICT observations. Both of these experiments use the 13.5-km domain to perform the ensemble forecast and data assimilation stages of the cycling and apply the nested 4.5-km domain when generating deterministic forecasts only. We then perform a third experiment (denoted "EnKF-4.5km") using the 4.5-km grid spacing nest during all stages of the cycling to examine the impact of increasing the resolution of the near-disturbance analyses. This experiment uses the same observations as the EnKF-PREDICT case and will be discussed separately from the two experiments that use a single 13.5-km grid spacing domain during data assimilation.

[1] The background error is estimated from 24- and 12-h forecast differences over the previous month using the National Meteorological Center (NMC) method (Parrish and Derber 1992). The calculation is performed using the gen_be utility in the WRF data assimilation package with control variable option 5.

3. Analysis results

a. Vortex evolution

This section compares the EnKF mean analyses for the MADIS and PREDICT experiments between 1200 UTC 10 September and 0000 UTC 18 September—a period that begins at the first flight mission time and ends on the last data assimilation cycle. In addition to providing initial conditions for deterministic and ensemble forecasts, these analyses are used as a dataset for studying the time evolution of the pregenesis disturbance. We use the region within 3° of the circulation center in the analyses to examine the kinematic structure of the disturbance from which Karl formed. The vortex center is determined objectively by first finding the center point that maximizes the azimuthal mean winds within 3° of the candidate locations at 950 and 700 hPa. The vortex center is then taken to be the average of these two estimates. If maximum 10-m winds exceed tropical storm strength ($18\,m\,s^{-1}$) in the model, a Barnes analysis (Barnes 1964) is performed using the 10-m, 850-hPa, and 700-hPa vorticity fields to find a wind-based storm center. This approach is similar to the Geophysical Fluid Dynamics Laboratory (GFDL) tracker algorithm (Marchok 2010) except that geopotential height and surface pressure data are omitted to avoid complications caused by land in the model.

We first examine the time series of mean relative vorticity near the storm center in the EnKF analyses, which was found in Munsell et al. (2013) to be an important factor in simulating intensity changes for Tropical Storm Erika (2009). Vertical relative vorticity (ζ) is averaged within 3° of the circulation center at 950 and 500 hPa (denoted $\overline{\zeta}$) to estimate the circulation strength at each time (Figs. 2a,b). A broad low-level vortex persists during the early assimilation cycles for each experiment, but decreases during 11−12 September; this is reflected in the 950-hPa $\overline{\zeta}$ in Fig. 2a. The dissipation of Karl on 17 September can also be seen from the rapid decrease in 950-hPa $\overline{\zeta}$ during the last assimilation cycles, when the simulated storm makes its second landfall on the coast of Mexico. Unlike the low-level vortex, the strength of the 500-hPa circulation increases steadily with time until the end of the cycling period (Fig. 2b). The decrease in the low-level circulation between 11 and 12 September and steady increase in the midlevel circulation are consistent with Fig. 8b of Davis and Ahijevych (2012), which shows the time evolution of average tangential winds estimated from the PREDICT dropsonde observations.

Observations of the pre-Karl disturbance reveal a large displacement of the low- and midlevel circulation centers in the days preceding genesis (Davis and Ahijevych

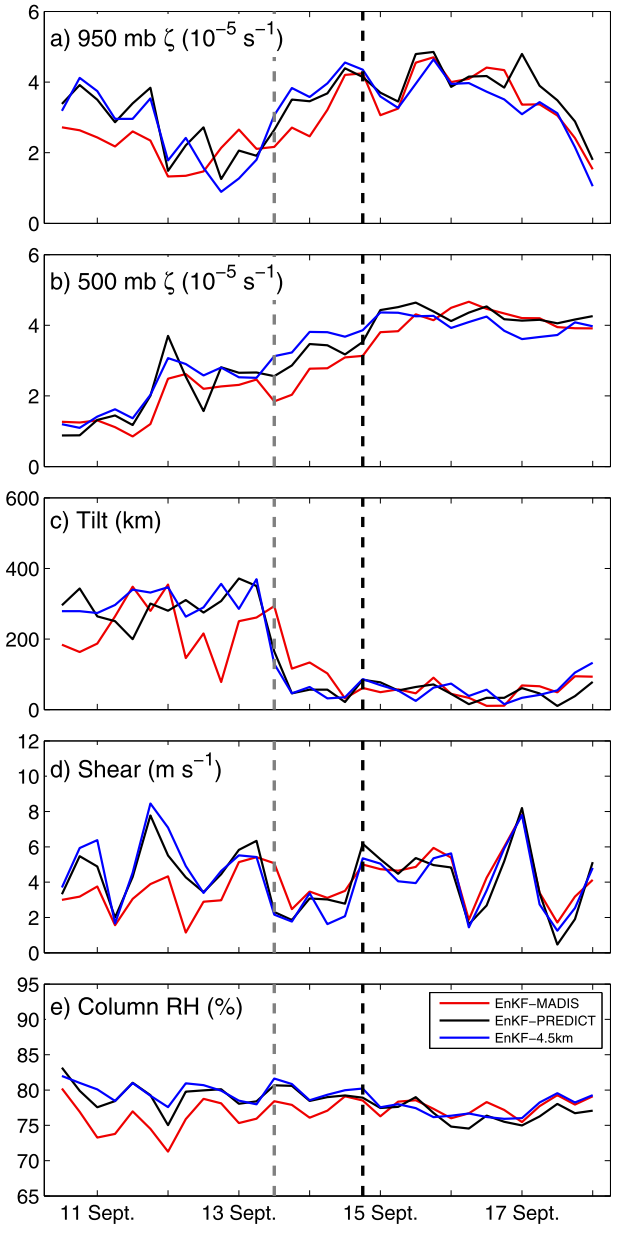

FIG. 2. (a) 950- and (b) 500-hPa relative vorticity, (c) 950–500-hPa tilt and (d) vertical shear, and (e) 950–500-hPa column relative humidity are plotted every 6 h for EnKF-MADIS (red), EnKF-PREDICT (black), and EnKF-4.5km (blue) analyses between 1200 UTC 10 Sep and 0000 UTC 18 Sep. The gray dashed line indicates the 1200 UTC 13 Sep cycle and the black dashed line indicates the time at which Karl became a tropical storm (1800 UTC 14 Sep).

2012). Likewise, the EnKF analyses in our experiment contain a large amount of vortex tilt, as defined by the difference between 950- and 500-hPa circulation centers (Fig. 2c). In Fig. 2d, we also plot the 950–500-hPa local vertical shear at each time, using winds within 3° of the storm center. The local shear takes into account the total effects of environmental shear and asymmetries induced by the tilted vortex. While the local shear is characterized by large fluctuations during the days leading up to genesis, the amplitude of these fluctuations decreases prior to 1800 UTC 14 September (indicated by the black dashed line in Fig. 2) as the low- and midlevel circulation centers reach a near vertical alignment (Fig. 2c). Mechanisms by which a tilted pregenesis vortex in vertical shear can realign are discussed in Schecter et al. (2002), Nolan and McGauley (2012), and Rappin and Nolan (2012), and are theorized to be an important factor in determining when tropical cyclogenesis will occur. Using idealized simulations, Rappin and Nolan (2012) show that the vertical alignment of the vortex (and eventual genesis) can be delayed substantially when the tilt is large. A large tilt can also increase the sensitivity of the genesis forecast to initial conditions, thus decreasing the intrinsic predictability of the event (Zhang and Tao 2013). For that matter, the vortex tilt in the analyses leading up to genesis is expected to have a large influence on the deterministic and ensemble forecasts, which will be discussed in sections 4 and 5. By including the PREDICT observations in the data assimilation cycles, the EnKF is able to spin up the midlevel vortex earlier in the cycling and produce a closer alignment between the 950- and 500-hPa circulations leading up to the genesis time.

b. *Thermodynamic structure*

Thermodynamic variables are compared in the vicinity of the tropical weather system for the same analyses described above. Figure 2e shows the 950–500-hPa column relative humidity (CRH, or the ratio of vertically integrated water vapor to vertically integrated saturation water vapor) averaged within 3° of the designated storm center. All cases show a clear diurnal cycle in CRH leading up to the genesis time. The pregenesis diurnal signal is consistent with Fig. 3b of Davis and Ahijevych (2012), which shows several daily maxima in cloud-top temperatures derived from Geostationary Operational Environmental Satellite (GOES) infrared data between 1200 and 1500 UTC. Melhauser and Zhang (2014) attribute this convective cycle to a nocturnal destabilization of the near-wave environment brought on by longwave radiative cooling. A similar diurnal signal is found in the 950–500-hPa shear (Fig. 2a), except that the daily maxima in shear typically occurs about 12 h after the maxima in CRH. In addition to the diurnal cycle in CRH, Fig. 2e shows an increase in mean CRH values near the center of the storm when PREDICT dropsondes are assimilated.

Average perturbation virtual potential temperature ($\overline{\theta_v'}$) is estimated by taking θ_v between 3° and 6° from the

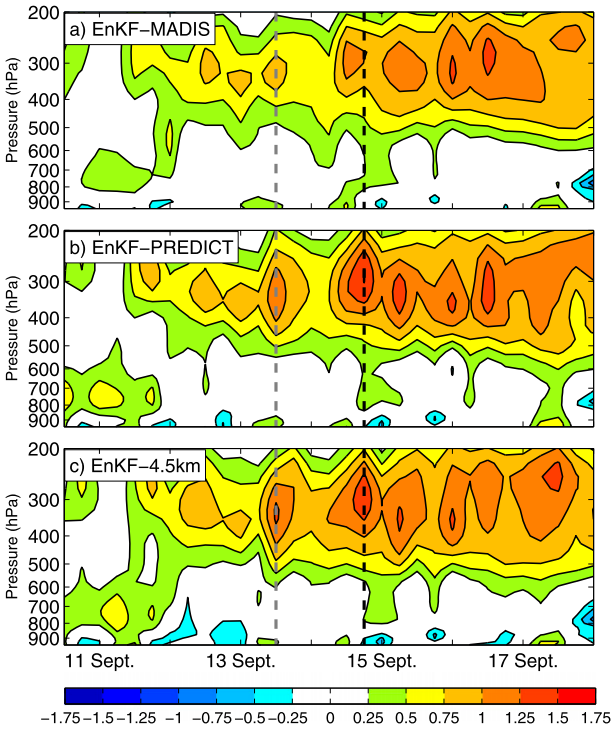

FIG. 3. Perturbation virtual potential temperature profiles for (a) EnKF-MADIS, (b) EnKF-PREDICT, and (b) EnKF-4.5km analyses are plotted every 6 h from 1200 UTC 10 Sep to 0000 UTC 18 Sep. The gray dashed line indicates the 1200 UTC 13 Sep cycle and the black dashed line indicates the time at which Karl became a tropical storm (1800 UTC 14 Sep).

center as the environmental value and subtracting it from the mean θ_v within 3° of the center. Vertical profiles are plotted every 6 h in Fig. 3 for the same analysis times shown in Fig. 2. Starting from 1200 UTC 11 September, both cases produce a warm θ_v anomaly above 600 hPa in the analyses. The upper-level warm anomaly increases steadily in the analyses leading up to genesis, but undergoes no major changes as Karl forms into a tropical storm prior to 15 September and rapidly intensifies during 16–17 September. Consistent with the higher 500-hPa circulation strength (Fig. 2d), the case that uses PREDICT observations yields larger perturbations to θ_v in the days leading up to genesis (Figs. 3b,c), suggesting that PREDICT observations help accelerate the development of the midlevel vortex.

4. Deterministic forecasts from EnKF analyses

a. Track and intensity

Deterministic forecasts are run from the 13.5-km EnKF mean analyses using a 4.5-km nested domain that follows the storm with the preset moves option in WRF (Figs. 4a–d). The location of the moving nest in the domain comes from 3-h position estimates of the tropical weather system that were determined from 13.5-km forecasts without the nest. Each simulation starts from the respective analysis time and ends shortly after the second landfall time at 0000 UTC 18 September. Results are shown for simulations that are initialized between 1800 UTC 12 September and 0000 UTC 15 September to compare the forecast performance in the 48 h leading up to genesis. Simulations that are initialized before 1800 UTC 12 September do not capture the vortex alignment that occurs in the analyses between 13 and 14 September (Fig. 2a). We omit forecast results from these times because of the inability of the model to generate a tropical cyclone by the end of the forecast period.

Starting from 1200 UTC 13 September, simulations that are initialized from EnKF analyses without PREDICT dropsondes provide reasonable track forecasts for Karl; that is, they reproduce the southern path of the storm over the Bay of Campeche and a second landfall on the Mexican coast before 18 September. These simulations also produce a tropical cyclone before the end of the forecast period, but have little skill in predicting the timing of genesis (Fig. 4b). Though not shown, the number of GOES cloud-top wind observations increases significantly in the vicinity of the tropical disturbance at 1200 UTC 13 September. The availability of new wind data over the weather system provides the EnKF with enough information to make accurate position updates to the midlevel circulation, which leads to the improved track forecasts after this time. In the absence of high-resolution in situ observations near the tropical weather system, the EnKF-MADIS case provides a storm structure that is not favorable for genesis until late in the simulations. The simulated disturbance is slow to develop in the forecasts, owing to the weak circulation and column moisture and a displacement (tilt) between the low- and midlevel circulation centers in the analyses (Fig. 2). The only deterministic forecast from these analyses that accurately predicts a landfalling tropical cyclone for the Yucatan Peninsula is initialized from 1200 UTC 14 September, 6 h before the true genesis event occurred.

Figures 4b and 4d show a large improvement in the intensity forecasts when PREDICT dropsondes are included in the set of assimilated observations. One benefit is that all forecasts that are generated after the 1800 UTC 12 September cycle capture the genesis event before making the second landfall on 17 September. Deterministic forecasts begin to accurately predict a landfalling tropical storm for the Yucatan Peninsula at 1200 UTC 13 September, which is a 24-h improvement over the control EnKF case in terms of ability to forecast the genesis event prior to landfall. These simulations more accurately

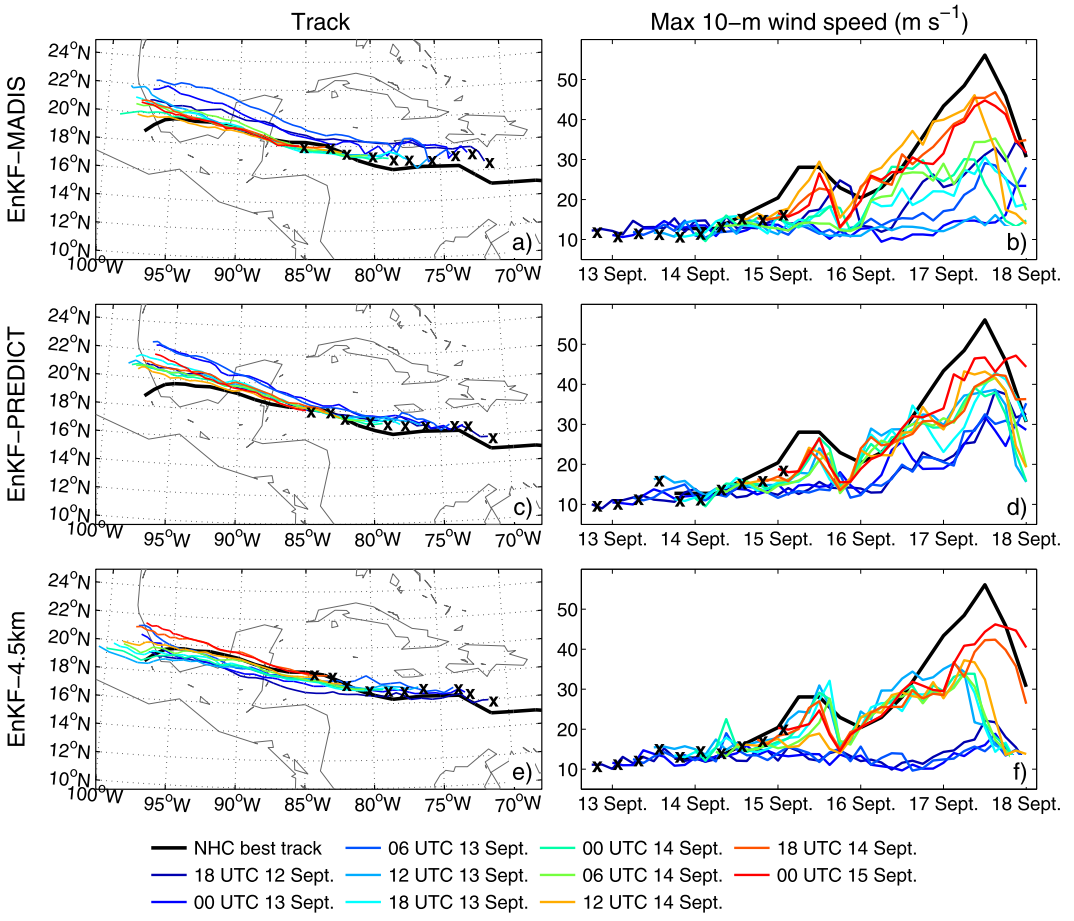

FIG. 4. Deterministic (left) track and (right) intensity forecasts from the (top) EnKF-MADIS, (middle) EnKF-PREDICT, and (bottom) EnKF-4.5km experiments. Forecasts are colored according to initialization time and NHC best-track data is plotted in black. The crosses in each panel indicate analysis values in the simulations.

reproduce the rapid intensification on 16 September as well, likely because a self-sustained tropical cyclone forms before entering the Bay of Campeche. The EnKF-PREDICT analyses also produce more accurate position estimates of the tropical system, indicated by the crosses in Fig. 4, which translates into improvements in the track forecasts during the early cycles. Because the EnKF maintains a full-physics ensemble of model states throughout the cycling, each analysis allows information from previous assimilation cycles to contribute to the flow-dependent background covariance used during the data assimilation. The analyses in the EnKF-PREDICT case therefore benefit from the additional observations as well as an improved background ensemble at each cycle.

Dropsondes from the PREDICT flight missions have a similar spatial coverage of the pregenesis disturbance at each time, so the increase in forecast performance after 1200 UTC 13 September is expected to come mostly from the changing dynamics of the pregenesis disturbance leading up to this data assimilation cycle; see Davis and Ahijevych (2012) for a detailed description of the dropsondes at each time.

b. *Forecasts from 0600 and 1200 UTC 13 September*

The EnKF-PREDICT experiment produces the first accurate deterministic forecast for the prelandfall genesis event on 1200 UTC 13 September. Forecast data from the 4.5-km grid spacing moving nest are used in this section to compare the vertical structure of the disturbance before and after genesis in the EnKF-MADIS and EnKF-PREDICT data assimilation experiments.

Figures 5a and 5b show the time series of 950- and 500-hPa mean relative vorticity every 3 h for forecasts initialized on 0600 and 1200 UTC 13 September from the pair of analyses. These results are compared with the EnKF-PREDICT analyses (green lines in Fig. 5), which represent the best estimate of Karl's kinematic and thermodynamic structure at each forecast time. While the 0600 UTC 13 September EnKF-PREDICT simulation is slow to

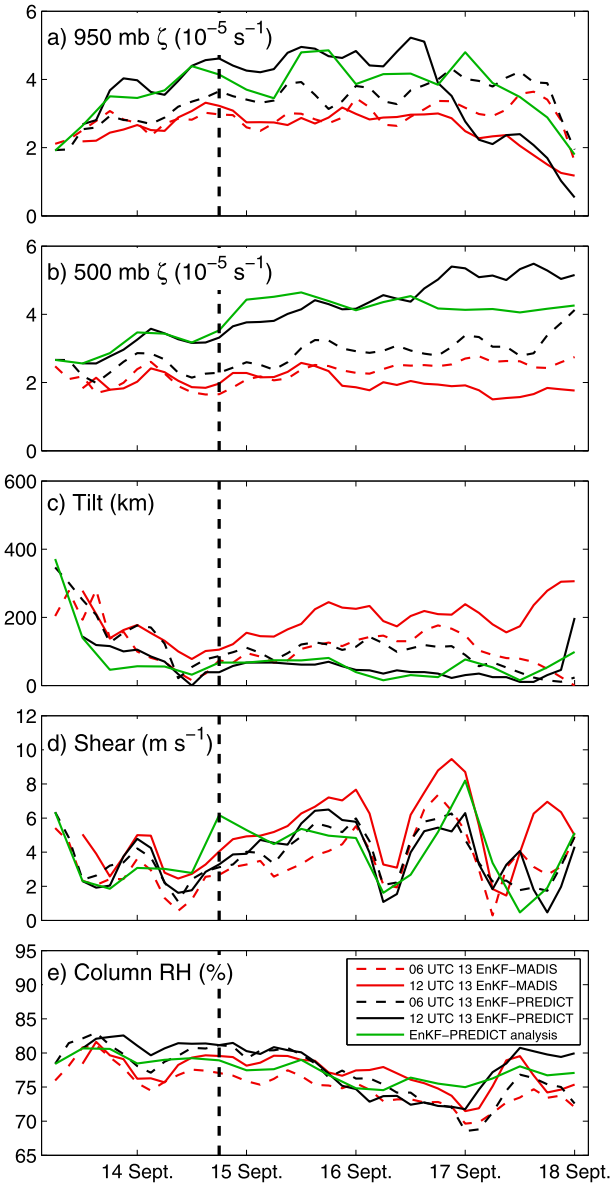

FIG. 5. (a) 950- and (b) 500-hPa relative vorticity, (c) 950–500-hPa tilt and (d) vertical shear, and (e) 950–500-hPa column relative humidity are plotted every 3 h for forecasts initialized at 0600 UTC (dashed red) and 1200 UTC 13 Sep (solid red) from the EnKF-MADIS analyses and 0600 UTC (dashed black) and 1200 UTC 13 Sep (solid black) from the EnKF-PREDICT analyses. The EnKF-PREDICT analyses are plotted in green every 6 h. The black dashed line indicates the time at which Karl became a tropical storm (18 UTC 14 Sep).

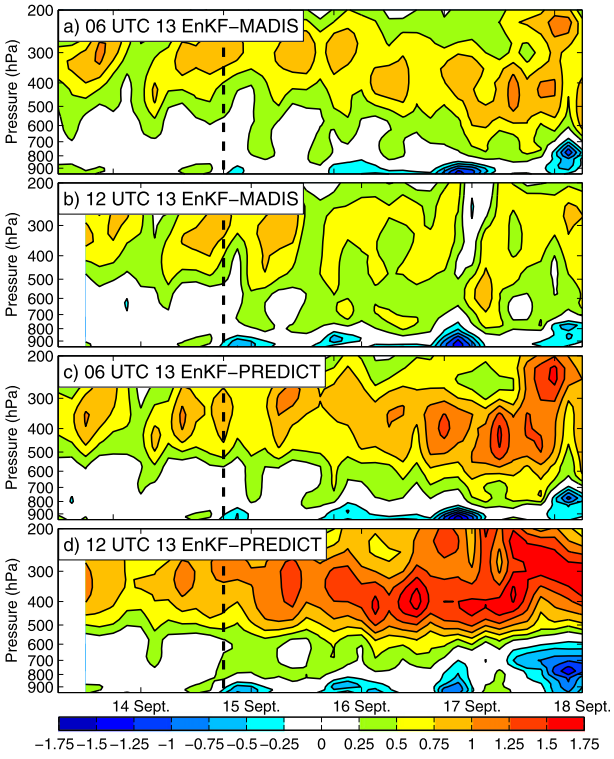

FIG. 6. Perturbation virtual potential temperature profiles are plotted every 3 h for forecast data initialized at (a) 0600 UTC and (b) 1200 UTC 13 Sep from the EnKF-MADIS analyses and at (c) 0600 UTC and (d) 1200 UTC 13 Sep from the EnKF-PREDICT analyses. The black dashed line indicates the time at which Karl became a tropical storm (18 UTC 14 Sep).

amplify the low-level vorticity, the 1200 UTC 13 forecast produces the same rapid increase in the surface vortex that is found in the analyses (Fig. 5a). Likewise, forecasts that are initialized from the EnKF-MADIS analyses are slow to increase the low- to midlevel circulation strength with time, thus showing the importance of the PREDICT observations at 1200 UTC 13 September. The stronger circulation aids the disturbance in retaining higher values of 950–500-hPa CRH during the hours leading up to genesis (Fig. 5e), which will be shown in section 5 to contribute greatly to Karl's genesis in ensemble forecasts.

The alignment of the low- and midlevel circulations in the analyses appears to be an important factor in simulating Karl's development (Figs. 5c,d). The vortex in the 0600 UTC 13 September EnKF-PREDICT determinstic forecast is initialized with a 370-km tilt, and intensifies slowly with time (Figs. 5a,b). Nevertheless, the accuracy of the genesis forecasts improves greatly after the vortex tilt in the analyses decreases to 140 km on 1200 UTC 13 September. All EnKF-PREDICT forecasts that are generated after the vortex alignment on 13 September capture the genesis and rapid intensification that follows (Fig. 4d). Despite the decrease in tilt after initialization for the four forecasts examined in Fig. 5, the local vertical shear remains relatively high after 0000 UTC 15 September because of an increase in vertical speed shear (not shown).

The stronger vortex that is produced in the EnKF-PREDICT forecasts coincides with a larger θ_v anomaly in the middle troposphere (Figs. 6c,d), owing to the

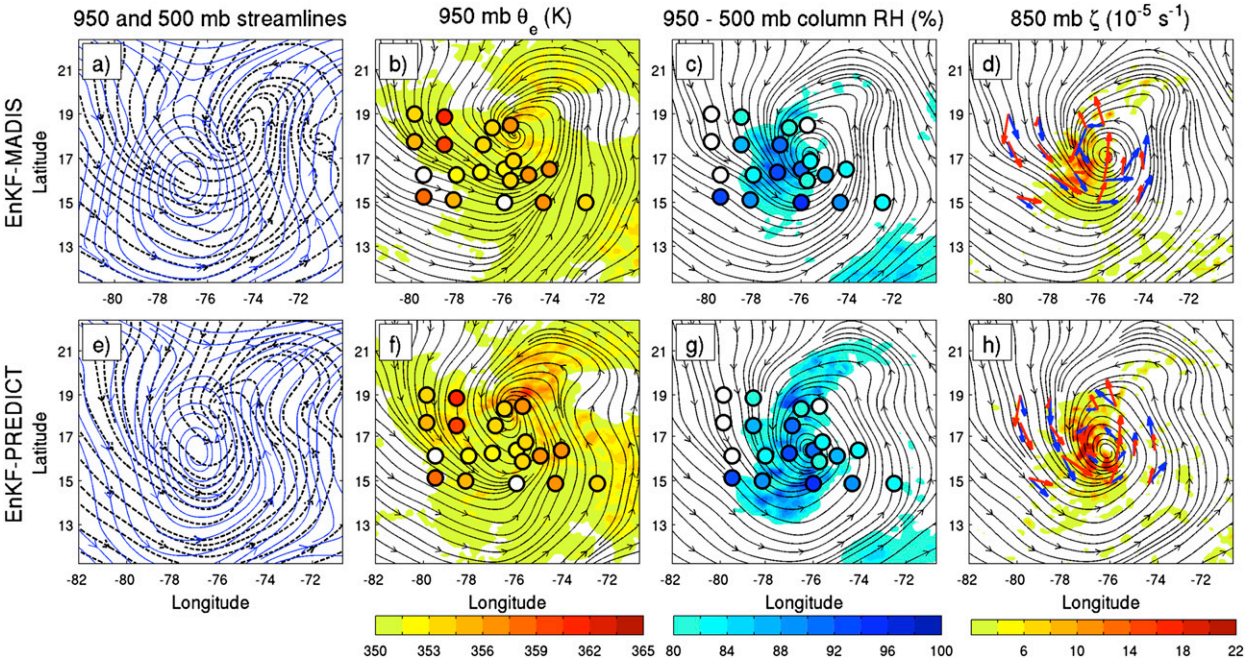

FIG. 7. (a)–(d) EnKF-MADIS and (e)–(h) EnKF-PREDICT analyses are compared at 1200 UTC 13 Sep. Streamlines are plotted at (a), (e) 950 (black dashed) and 500 (blue), (b),(f) 950 and (c),(d),(g),(h) 850 hPa. (b),(f) Equivalent potential temperature, (c),(g) column relative humidity, and (d),(h) 850-hPa vertical relative vorticity are shaded in 1.5-K, 2%, and $2 \times 10^{-5}\,s^{-1}$ increments, respectively. Shaded circles in (b),(c),(f),(g) indicate values calculated from PREDICT observations. PREDICT wind vectors (red) are plotted in (d),(h) along with filtered analysis wind vectors (blue) at the dropsonde locations.

development of a balanced system-scale vortex in the forecasts. The magnitudes of the θ_v anomalies are greater for the forecast data than the analysis data (comparing Figs. 3 and 6) likely because the model is allowed to simulate the amplification of the system-scale disturbance and eventual genesis event with no discontinuities from the data assimilation. This is demonstrated in the EnKF-PREDICT case by the large increase in upper-level $\overline{\theta_v'}$ during rapid intensification on 16 September (Fig. 6d). These simulations also produce strong negative perturbations in surface θ_v during the late afternoon to evening hours (1800–0000 UTC), which appear as a much weaker signal in the analysis $\overline{\theta_v'}$ fields. The negative perturbations reflect large-scale warming away from the storm (cf. Melhauser and Zhang 2014) and not a decrease of θ_v in the low-level vortex at these times. The diurnal signal persists throughout the entire length of the simulations, but it appears more strongly in $\overline{\theta_v'}$ as the tropical cyclone intensifies and causes the inner 3° of the verification region to become less sensitive to diurnal changes in radiation.

c. *The development of Karl in the 1200 UTC 13 September simulations*

Figure 7 provides a more detailed comparison of the 1200 UTC 13 September analyses with and without the PREDICT observations. Each plot uses system-relative streamlines to show the flow field following the pregenesis disturbance. The streamlines are estimated by subtracting a 6-h storm-motion vector from each wind field. A two-dimensional low-pass filter is then used to remove wavelengths smaller than 150 km to compare the "system scale" winds near the disturbance. The EnKF-MADIS case produces a 500-hPa vortex near the same location as in the EnKF-PREDICT case (Figs. 7a,e). Nevertheless, the 950-hPa vortex is located much farther behind the 500-hPa cyclone in the EnKF-MADIS analysis. The close agreement between the 500-hPa vortex locations in the two experiments may be due to the availability of GOES wind vectors at this time (not shown), though the circulation of the midlevel cyclone is much greater when the PREDICT observations are included (Fig. 5d). The 850-hPa streamlines and unfiltered ζ are plotted in Figs. 7d and 7h along with system-relative wind vectors from the analyses and PREDICT dropsondes. The comparison between observed and analysis wind vectors at this time verifies the larger vortex position error in the EnKF-MADIS case, and demonstrates the role of PREDICT observations in representing the low-level circulation beneath the midlevel vortex. These wind vectors also indicate that the position of the vortex in the EnKF-PREDICT analysis remains displaced westward of the true vortex position at this time, despite the assimilation

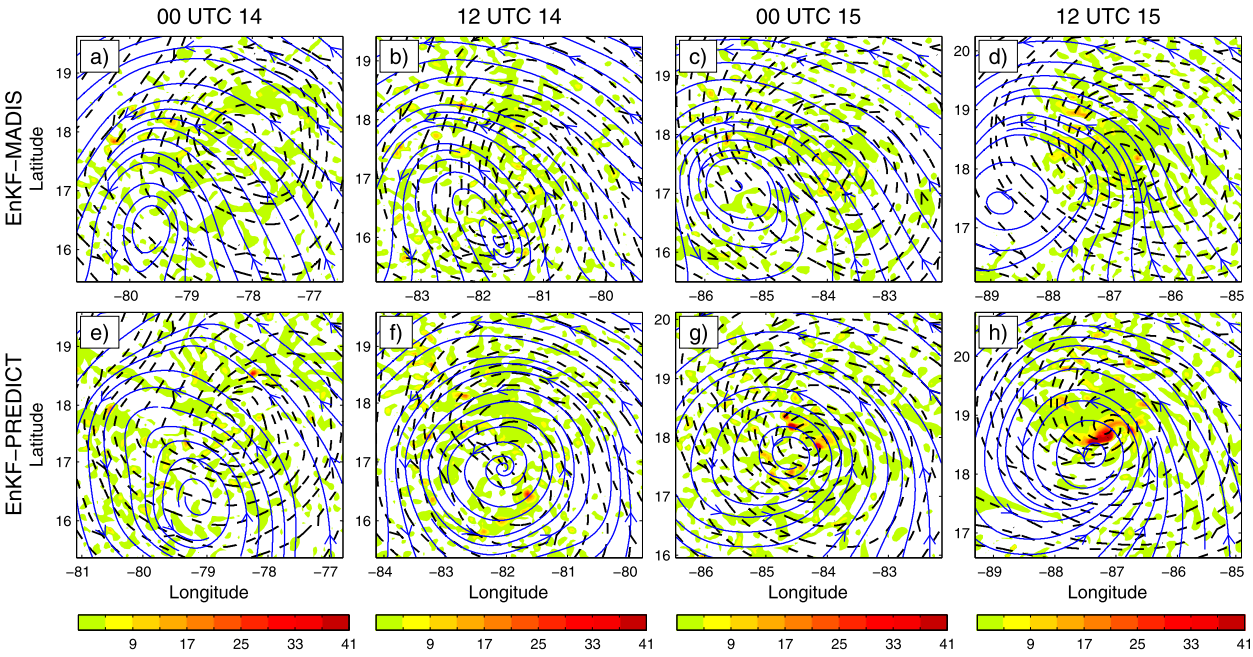

FIG. 8. Forecasts initialized from the (a)–(d) EnKF-MADIS and (e)–(h) EnKF-PREDICT analyses at 1200 UTC 13 Sep are compared. Filtered system-relative streamlines are plotted every 12 h from 0000 UTC 14 Sep to 1200 UTC 15 Sep at 950 (black dashed) and 500 hPa (blue). The 950-hPa relative vorticity is shaded every $4 \times 10^{-3}\,s^{-1}$ from $2 \times 10^{-3}\,s^{-1}$.

of additional observations. When performing the data assimilation, the EnKF relies on a sparse set of observations, relative to the state space, and imperfect estimates of forecast error covariance to move the vortex and correct its intensity. Nevertheless, the resulting analysis reproduces several features of the pregenesis disturbance that favor Karl's future genesis, even if the position of the system-scale vortex is imperfect.

In addition to capturing the low- and midlevel vortex alignment, the EnKF-PREDICT analysis contains higher equivalent potential temperature (θ_e) and CRH near the low-level circulation (Figs. 5b,c,f,g), which favors organized deep convection near the surface low. The EnKF-MADIS case contains relatively high values of CRH in the southwest portion of the cyclone, but most of the eastern part of the circulation is exposed to dry air at this time. Both sets of analyses contain slightly lower-than-observed CRH away from the main circulation center when verified with the PREDICT dropsondes (shaded circles in Figs. 5c,g). The presence of dry air within the storm-relative recirculation region may have slowed the early development of Karl in the EnKF-PREDICT simulations, causing the 18-h lag in forecasting tropical-storm-force winds for simulations that are initialized between 1200 UTC 13 September and 1800 UTC 14 September.

Forecasts that are initialized from the two EnKF analyses in Fig. 7 are compared in Fig. 8. Genesis occurs near 1200 UTC 15 September in the simulation that is initialized from the EnKF-PREDICT analysis, while the EnKF-MADIS case fails to produce a tropical cyclone during the same forecast period. Filtered system-relative streamlines are plotted every 12 h from 0000 UTC 14 September to 1200 UTC 15 September at 950 and 500 hPa along with positive values of unfiltered 950-hPa ζ. The 950-hPa circulation in the EnKF-MADIS forecast remains weak after initialization (Fig. 5c) and lags behind the midlevel circulation in the days leading up to the genesis time. Likewise, the 950-hPa circulation in the EnKF-PREDICT simulation moves closer to the 500-hPa cyclone and intensifies with time. The forecast from this analysis also contains a noticeably higher number of mesoscale vorticity anomalies 24 h into the simulation that increase in size as the simulation approaches the genesis time.

A scale separation of the 950-hPa vorticity and divergence is performed on the forecast data to compare the development of the low-level cyclone before and after genesis in the two cases. As in Fang and Zhang (2011), the scales are organized into three categories: the main system-scale vortex ($L > 150$ km), the intermediate or cluster scale ($50 < L < 150$ km), and the cloud scale, which is made up of individual convective cells ($L < 50$ km). The spectral energy (amplitude) of the scale-separated vorticity and divergence is averaged within 3° of the circulation center every 3 h from the 4.5-km nested domain. Figure 9 compares the amplitude

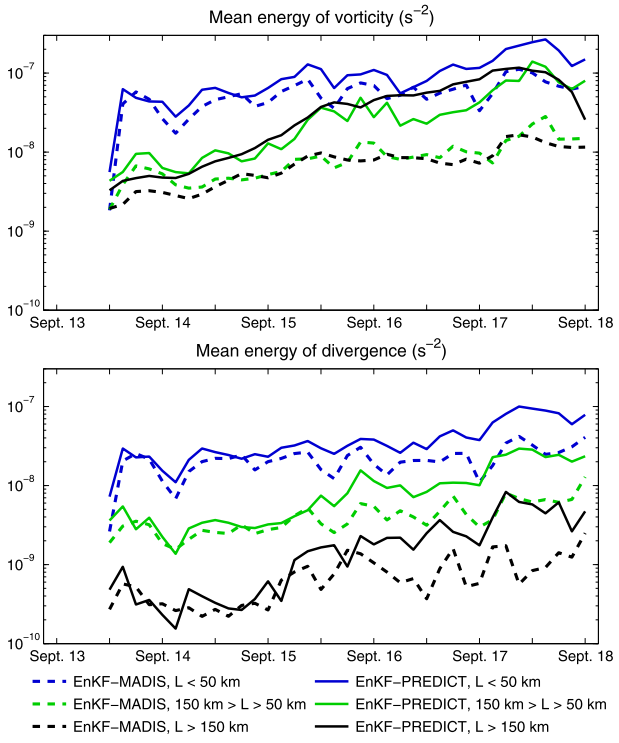

FIG. 9. Mean spectral energy in the system-scale ($L > 150$ km), intermediate-scale ($50 > L > 150$ km), and small-scale ($L < 50$ km) (top) vorticity and (bottom) divergence is plotted for forecast data initialized from the 1200 UTC 13 Sep (dashed lines) EnKF-MADIS and (solid lines) EnKF-PREDICT analyses.

changes in the vorticity and divergence fields over time. While the amplitudes undergo many fluctuations throughout the forecast period, the vorticity and divergence steadily increase with time until the last hours of the simulation, owing to an increase in positive vorticity and convergence. Both forecasts produce a large spike in the initial convective-scale energy as the model adjusts to instabilities that are introduced during the data assimilation. After the initial adjustment, the energy in the convective-scale vorticity increases slowly to the end of the forecast period. Likewise, the energy in the intermediate- and system-scale vorticity also amplifies over the forecast period. The EnKF-PREDICT simulation, however, strengthens the larger-scale vorticity field at a faster rate than the EnKF-MADIS case. In the first 48 h of the EnKF-PREDICT simulation, the energy in the vorticity field increases at a rate that is unmatched by the divergence field; that is, the flow becomes increasingly more rotational leading up to genesis. Fang and Zhang (2011) propose that the development of the low-level vortex follows from the convergence of large-scale or convectively generated vorticity toward the center of the system-scale cyclone. For the development of Hurricane Dolly (2008), they showed that the Rossby radius of deformation could decrease to values that are smaller or comparable to the system scale as the low-level vortex intensifies. The convective-scale diabatic heating can be effectively trapped by the system-scale circulation in the pregenesis disturbance as the flow in the system-scale vortex approaches geostrophic balance. The two simulations compared in Fig. 9 contain minor differences in the early production of small-scale vorticity, owing to the larger column moisture in the EnKF-PREDICT simulation. Nevertheless, the initial intermediate- and system-scale vorticity in these two cases differ by a factor of 2. The EnKF-MADIS simulation appears to lack a sufficiently strong system-scale circulation to protect the near-wave air from the relatively dry environment (Dunkerton et al. 2009) or, as described by Fang and Zhang (2011), organize the small- and intermediate-scale vorticity anomalies and amplify the system-scale vortex. This can be seen from the lack of intermediate-scale development and the smaller production of vorticity at the cloud scale in the EnKF-MADIS forecast. Though not shown, this is also true for forecasts that are initialized prior to 1200 UTC 13 September that did not capture the genesis before the initial landfall.

5. Ensemble forecasts from EnKF analyses

One conclusion from the cycling data assimilation experiments is that deterministic forecasts that are initialized before 1200 UTC 13 September fail to produce the genesis event in the EnKF-PREDICT case. Using ensemble forecasts from 1200 UTC 12 September, Torn and Cook (2013) found the development of Karl to be most sensitive to the initial circulation in the lower troposphere. For that matter, we hypothesize that the stronger low-level circulation induced by the PREDICT observations at this cycle creates conditions that are more favorable for genesis. To investigate this result, ensemble forecasts are run from 0600 and 1200 UTC 13 September to quantify changes in the probabilistic forecasts before and during the first cycle that successfully predicts the genesis event. These forecasts are initialized from the 13.5-km EnKF-MADIS and EnKF-PREDICT analyses and do not use a 4.5-km nested domain. To distinguish between developing and nondeveloping members, we define a developing member to be a simulation that contains maximum 10-m winds $> 18\,\mathrm{m\,s^{-1}}$ (tropical storm strength) for three consecutive 3-h time stamps between 1800 UTC 14 September and 0000 UTC 16 September. This criterion limits the developing cases to members that form and maintain a tropical cyclone before making landfall on the Yucatan Peninsula.

The EnKF-MADIS and EnKF-PREDICT ensemble analyses at 0600 UTC 13 September produce a similar

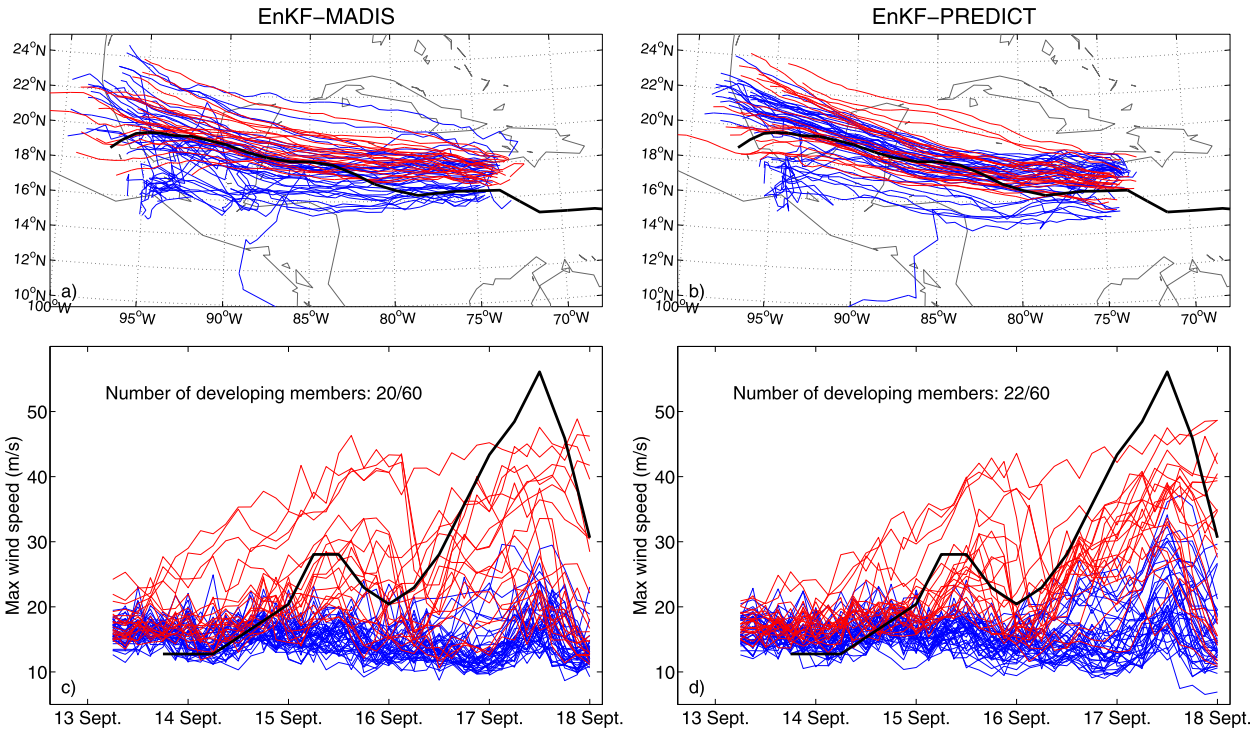

FIG. 10. Ensemble (a),(b) track and (c),(d) intensity forecasts are shown for the (left) EnKF-MADIS and (right) EnKF-PREDICT experiments. Each ensemble is initialized at 0600 UTC 13 Sep and runs to 0000 UTC 18 Sep. Developing members are plotted in red, nondeveloping members are blue, and the best-track data is plotted in black.

number of developing forecast members (20 and 22, respectively) as indicated by the red (developing) and blue (nondeveloping) lines in Fig. 10. While a larger intensity spread is observed for the case that does not use the PREDICT observations, the two ensembles provide similar probabilistic forecasts for genesis at this time. The ensemble forecasts suggest that a potential for genesis exists, even before the deterministic forecasts predict Karl's development. In the next analysis cycle at 1200 UTC 13 September, the number of developing members for the EnKF-MADIS case increases from 20 to 26, while the developing members in the EnKF-PREDICT case increases more substantially from 22 to 44 (comparing Figs. 10 and 11). The change in genesis probability between 0600 and 1200 UTC therefore agrees with the deterministic forecast results in Fig. 4. As mentioned earlier, a larger-than-average number of upper-level satellite winds are available during the 1200 UTC 13 September cycle, which may have contributed to the modest increase in predictability at this time for the EnKF-MADIS case. Nevertheless, the large increase in genesis probability for the EnKF-PREDICT case comes mostly from additional dropsondes that were collected from a midday flight mission on 13 September. Both of these factors may have also led to the observed reduction in storm track uncertainty in these analyses and forecasts.

The field observations were shown in the previous sections to increase the system-scale circulation at low to midlevels of the ensemble-mean analysis, which contributes to the development of the tropical cyclone in the deterministic forecast. To understand how this result affects the ensemble forecasts, vertical profiles of system-scale mean ζ are estimated for the EnKF-PREDICT ensemble to compare the circulation strength between developing and nondeveloping members. A two-dimensional low-pass filter is applied to remove features with wavelengths smaller than 150 km from the ζ field, and values are averaged within 3° of the circulation center every 25 hPa from the surface to 500 hPa. The mean ζ profiles are plotted for ensemble members at the 0600 and 1200 UTC 13 September analysis times (Figs. 12a,c) and for the 6-h ensemble forecast from 0600 UTC 12 September (Fig. 12b). As in Figs. 10 and 11, the red and blue lines indicate the developing and nondeveloping members, respectively. In agreement with the deterministic forecasts, members that are initialized with larger system-scale circulation between the surface and 600 hPa are more likely to produce a tropical cyclone before the first landfall time. The increase in mean

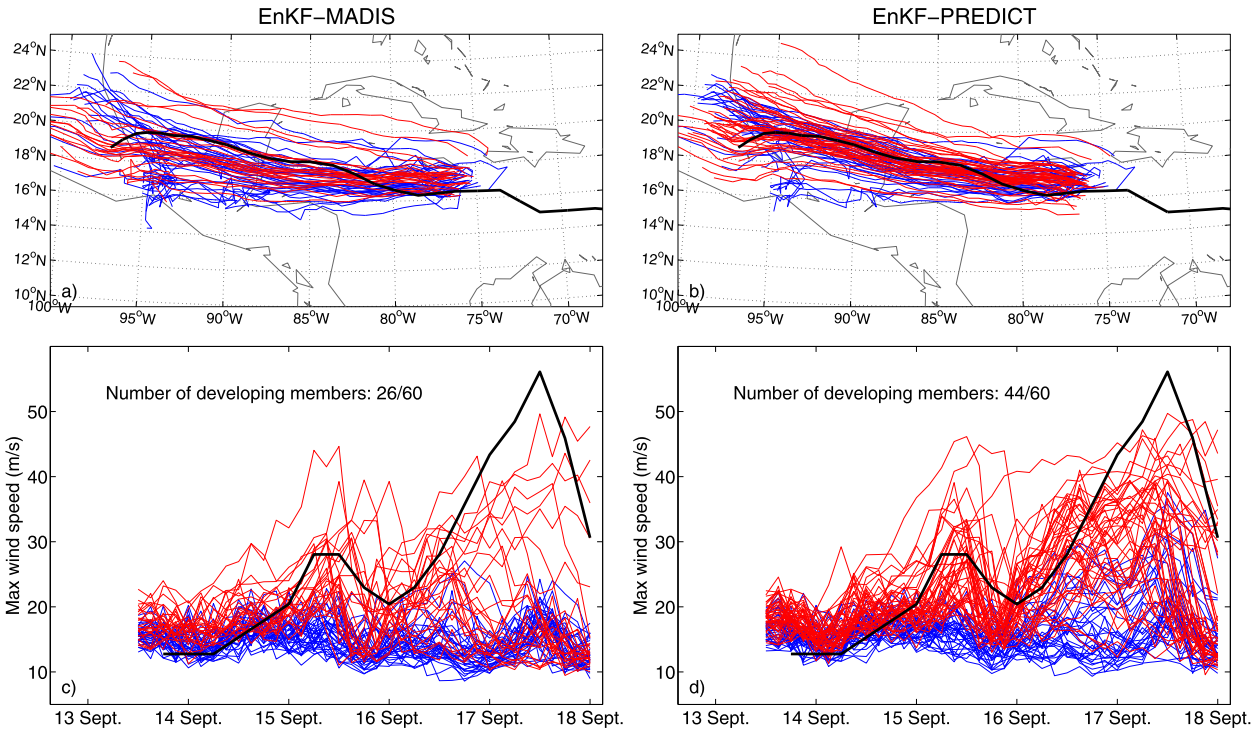

FIG. 11. Ensemble (a),(b) track and (c),(d) intensity forecasts are shown for the (left) EnKF-MADIS and (right) EnKF-PREDICT experiments. Each ensemble is initialized at 1200 UTC 13 Sep and runs to 0000 UTC 18 Sep. Developing members are plotted in red, nondeveloping members are blue, and the best-track data is plotted in black.

ζ going from 0600 to 1200 UTC 13 September is most substantial below 700 hPa in the ensemble members, where the PREDICT observations are assumed to have the largest impact, owing to the lack of low-level satellite winds. It is also worth noting that the spinup of the low-level cyclone using PREDICT dropsondes is inherently linked to vortex tilt, as the strong 950-hPa vortices in the EnKF-PREDICT ensemble analyses are located close to the 500-hPa center at this time (Fig. 7).

6. Impact of model resolution on EnKF analyses and forecasts

This section describes a third data assimilation experiment that examines the effects of model resolution on the EnKF analyses. We repeated the EnKF-PREDICT case using a nested 253 × 253 domain with 4.5-km grid spacing during the ensemble forecast and analysis steps of the data assimilation cycles (denoted EnKF-4.5km). Given that 4.5-km grid spacing can more accurately represent the effects of convective-scale features in the model, our early hypothesis was that a high-resolution ensemble might improve the background error covariance estimate between cycles, thus making the data assimilation more effective.

To verify the high-resolution analysis results, the time series of 950–500 hPa shear, tilt, CRH, and average ζ are compared with analyses from the previous two experiments in Fig. 2. The higher resolution data assimilation has little noticeable effects on the location and magnitude of the low- and midlevel circulation leading up to genesis, and obtains the same estimate of integrated moisture near the circulation center as the lower-resolution EnKF-PREDICT case. While the EnKF-4.5km experiment produces a slightly larger upper-level θ_v anomaly in the storm center before and after genesis (Fig. 3c), the differences in thermodynamic structure remain relatively small between the two PREDICT cases. Likewise, the higher-resolution data assimilation produces little improvement in deterministic track and intensity forecasts leading up to genesis (Figs. 4e,f). It follows that the model resolution used in the EnKF-MADIS and EnKF-PREDICT experiments is sufficient for capturing the features of the pregenesis disturbance and surrounding environment that lead to the formation of Karl. This result is not surprising, considering that the role of vorticity at scales larger than the convective and intermediate scales was shown in Figs. 9 and 12 to be instrumental to Karl's development. The accuracy of the analyses may also be limited to the meso-α or meso-β scales in our experiments,

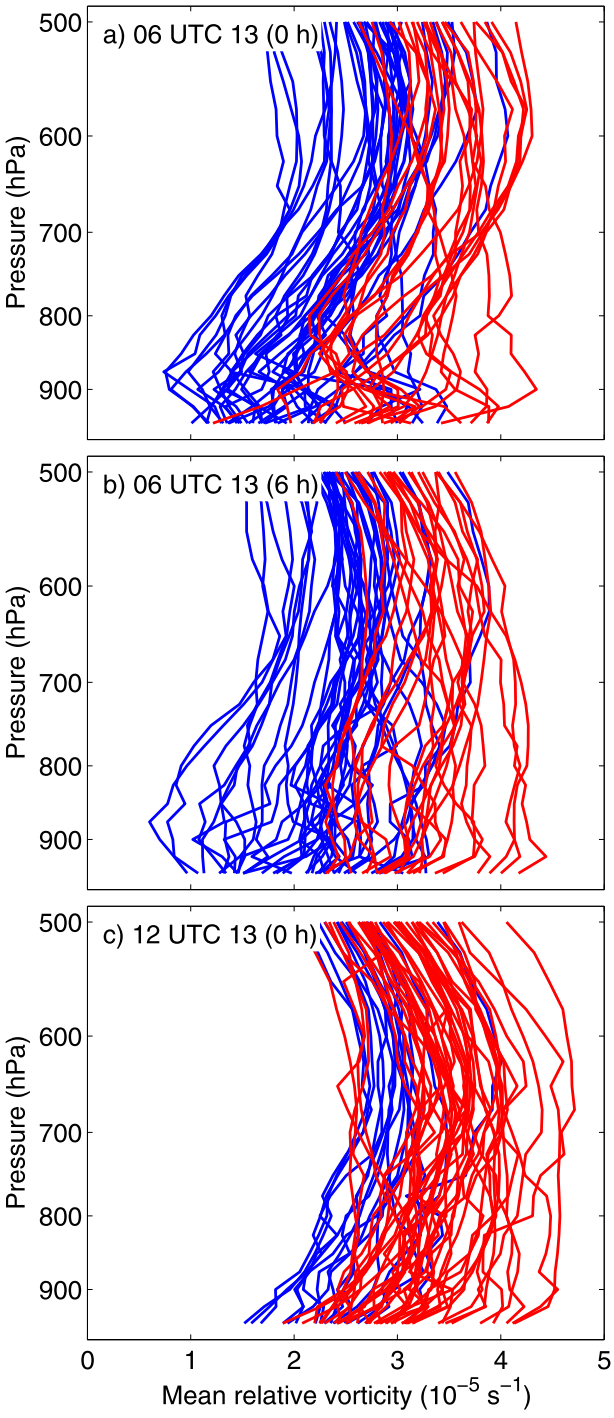

FIG. 12. Vertical profiles of relative vorticity averaged within 3° of the circulation center for the EnKF-PREDICT members. Values are plotted for (a) the 0600 UTC 13 Sep ensemble analyses, (b) the 6-h forecasts from the 0600 UTC 13 Sep ensemble analyses, and (c) the 1200 UTC 13 Sep ensemble analyses.

given the spatial and temporal frequency of observations and possible limitations in the applied data assimilation method.

7. Conclusions

This study investigates the predictability of a tropical cyclogenesis event using an EnKF data assimilation system that was applied in real time during the PREDICT field campaign. Cycling data assimilation experiments are performed over a 10-day period in which Hurricane Karl formed, rapidly intensified into a category-3 hurricane, and dissipated over the Mexican coast. One set of analyses uses routinely collected observations from MADIS, while a second set uses both MADIS and PREDICT observations. The EnKF analyses that take into account PREDICT dropsondes provide a detailed four-dimensional dataset, which is used for examining the factors that led to Karl's genesis. Deterministic and ensemble forecasts from these analyses are also used to examine the role of initial-condition errors in predicting genesis.

Our results show that the PREDICT observations improve significantly the conditions for genesis in the analyses. The additional dropsonde measurements increase the system-scale vortex strength in the lower and middle levels while reducing the displacement between the low- and midlevel circulation centers. They also produce larger warm-temperature anomalies in the system-scale vortex and increase the integrated moisture between 950 and 500 hPa. These factors yield a 24-h increase in lead time for predicting the genesis of Karl from deterministic forecasts. The largest change in Karl's predictability occurs at 1200 UTC 13 September during cycling, owing to the alignment of the low- and midlevel cyclones and the strength of the low-level circulation in the ensemble-mean analyses. A PREDICT flight mission at this time provided the additional observations that were necessary for improving the deterministic and probabilistic forecasts for the genesis event. While the largest contribution of these observations is found at the mesoscale, synoptic-scale differences between our data assimilation experiments cannot be ruled out, given the spatial coverage of the dropsondes and the 900-km radius of influence that is used by the EnKF.

We performed an additional data assimilation experiment to examine the impact of model grid spacing on analyses near the tropical weather system. This experiment uses a configuration that is identical to the previous experiments, except that a nested 4.5-km grid spacing domain is applied during the ensemble forecast and analysis steps of the cycling. The nested analyses yield marginal

changes in the kinematic and thermodynamic structure of the disturbance but no systematic improvements in the deterministic forecasts for the genesis event. This result suggests that initial-condition errors at the meso-α or meso-β scales still pose large challenges for predicting genesis. We suspect that an improved observation network or targeted observations of the pregenesis disturbance can decrease the initial condition errors at these scales. Advanced four-dimensional or hybrid data assimilation methods and more efficient assimilation of remotely sensed observations may also be required before large gains can be made in predicting when and where tropical cyclones form.

Acknowledgments. This work was supported in part by the NOAA Hurricane Forecast Improvement Project (HFIP), Office of Naval Research Grant N000140910526 and the National Science Foundation Grant ATM-0840651. The computing was performed at the Texas Advanced Computing Center. We are thankful for the comments provided by three anonymous reviewers for improving the manuscript.

REFERENCES

Barnes, S. L., 1964: A technique for maximizing details in numerical weather map analysis. *J. Appl. Meteor.,* **3,** 396–409.

Bister, M., and K. A. Emanuel, 1997: The genesis of Hurricane Guillermo: TEXMEX analyses and a modeling study. *Mon. Wea. Rev.,* **125,** 2662–2682.

Davis, C. A., and D. A. Ahijevych, 2012: Mesoscale structural evolution of three tropical weather systems observed during PREDICT. *J. Atmos. Sci.,* **69,** 1284–1305.

Dudhia, J., 1989: Numerical study of convection observed during the Winter Monsoon Experiment using a mesoscale two-dimensional model. *J. Atmos. Sci.,* **46,** 3077–3107.

Dunkerton, T. J., M. T. Montgomery, and Z. Wang, 2009: Tropical cyclogenesis in a tropical wave critical layer: Easterly waves. *Atmos. Chem. Phys.,* **9,** 5587–5646.

Evensen, G., 1994: Sequential data assimilation with a nonlinear quasi-geostrophic model using Monte Carlo methods to forecast error statistics. *J. Geophys. Res.,* **99** (C5), 10 143–10 162.

Fang, J., and F. Zhang, 2010: Initial development and genesis of Hurricane Dolly (2008). *J. Atmos. Sci.,* **67,** 655–672.

——, and ——, 2011: Evolution of multiscale vortices in the development of Hurricane Dolly (2008). *J. Atmos. Sci.,* **68,** 103–122.

Gaspari, G., and S. E. Cohn, 1999: Construction of correlation functions in two and three dimensions. *Quart. J. Roy. Meteor. Soc.,* **125,** 723–757.

Halverson, J., and Coauthors, 2007: NASA's Tropical Cloud Systems and Processes experiment: Investigating tropical cyclogenesis and hurricane intensity change. *Bull. Amer. Meteor. Soc.,* **88,** 867–882.

Hendricks, E. A., M. T. Montgomery, and C. A. Davis, 2004: The role of vortical hot towers in the formation of Tropical Cyclone Diane (1984). *J. Atmos. Sci.,* **61,** 1209–1232.

Hong, S.-Y., J. Dudhia, and S.-H. Chen, 2004: A revised approach to ice microphysical processes for the bulk parameterization of cloud and precipitation. *Mon. Wea. Rev.,* **132,** 103–120.

Marchok, T., cited 2010: Use of the GFDL vortex tracker. [Available online at http://www.dtcenter.org/HurrWRF/users/docs/presentations/tutorial02222010/tracker_slides.pdf.]

Melhauser, C., and F. Zhang, 2014: Diurnal radiation cycle impact on the pregenesis of Hurricane Karl (2010). *J. Atmos. Sci.,* in press.

Meng, Z., and F. Zhang, 2008a: Test of an ensemble Kalman filter for mesoscale and regional-scale data assimilation. Part III: Comparison with 3DVAR in a real-data case study. *Mon. Wea. Rev.,* **136,** 522–540.

——, and ——, 2008b: Test of an ensemble Kalman filter for mesoscale and regional-scale data assimilation. Part VI: Performance over a warm season month of June 2003. *Mon. Wea. Rev.,* **136,** 3671–3682.

Mlawer, E. J., S. J. Taubman, P. D. Brown, M. J. Iacono, and S. A. Clough, 1997: Radiative transfer for inhomogeneous atmospheres: RRTM, a validated correlated-k model for the longwave. *J. Geophys. Res.,* **102** (D14), 16 663–16 682.

Monin, A. S., and A. M. Obukhov, 1954: Basic laws of turbulent mixing in the surface layer of the atmosphere. *Tr. Geofiz. Inst., Akad. Nauk SSSR,* **24,** 163–187.

Montgomery, M. T., M. E. Nicholls, T. A. Cram, and M. E. Saunders, 2006: A vortical hot tower pathway to tropical cyclogenesis. *J. Atmos. Sci.,* **63,** 355–386.

——, and Coauthors, 2012: The Pre-Depression Investigation of Cloud-Systems in the Tropics (PREDICT) experiment. *Bull. Amer. Meteor. Soc.,* **93,** 153–172.

Munsell, E. B., F. Zhang, and D. P. Stern, 2013: Predictability and dynamics of a nonintensifying tropical storm: Erica (2009). *J. Atmos. Sci.,* **70,** 1849–1873.

Noh, Y., W.-G. Cheon, and S.-Y. Hong, 2003: Improvement of the K-profile model for the planetary boundary layer based on large eddy simulation data. *Bound.-Layer Meteor.,* **107,** 401–427.

Nolan, D. S., and M. G. McGauley, 2012: Tropical cyclogenesis in wind shear: Climatological relationships and physical processes. *Cyclones: Formation, Triggers and Control,* K. Oouchi and H. Fudeyasu, Eds., Nova Science Publishers, 1–34.

Parrish, D. F., and J. C. Derber, 1992: The National Meteorological Center's spectral statistical-interpolation analysis system. *Mon. Wea. Rev.,* **120,** 1747–1763.

Poterjoy, J., F. Zhang, and T. Weng, 2014: The effects of sampling errors on the EnKF assimilation of inner-core hurricane observations. *Mon. Wea. Rev.,* **142,** 1609–1630.

Rappin, E. D., and D. S. Nolan, 2012: The effect of vertical shear orientation on tropical cyclogenesis. *Quart. J. Roy. Meteor. Soc.,* **138,** 1035–1054.

Reasor, P. D., M. T. Montgomery, and L. F. Bosart, 2005: Mesoscale observations of the genesis of Hurricane Dolly (1996). *J. Atmos. Sci.,* **62,** 3151–3171.

Ritchie, E. A., and G. J. Holland, 1997: Scale interactions during the formation of Typhoon Irving. *Mon. Wea. Rev.,* **125,** 1377–1396.

Schecter, D. A., M. T. Montgomery, and P. D. Reasor, 2002: A theory for the vertical alignment of a quasigeostrophic vortex. *J. Atmos. Sci.,* **59,** 150–168.

Simpson, J., E. A. Ritchie, G. J. Holland, and J. Halverson, 1997: Mesoscale interactions in tropical cyclone genesis. *Mon. Wea. Rev.,* **125,** 2643–2661.

Sippel, J. A., and F. Zhang, 2008: A probabilistic analysis of the dynamics and predictability of tropical cyclogenesis. *J. Atmos. Sci.,* **65,** 3440–3459.

——, and ——, 2010: Factors affecting the predictability of Hurricane Humberto (2007). *J. Atmos. Sci.,* **67,** 1759–1778.

Skamarock, W. C., and Coauthors, 2008: A description of the Advanced Research WRF version 3. NCAR Tech. Note NCAR/TN-475+STR, 113 pp. [Available online at http://www.mmm.ucar.edu/wrf/users/docs/arw_v3_bw.pdf.]

Stewart, S. R., 2010: Tropical cyclone report Hurricane Karl (AL1312010) 14-18 September 2010. National Hurricane Center Tech. Rep., 17 pp. [Available online at http://www.nhc.noaa.gov/pdf/TCR-AL132010_Karl.pdf.]

Torn, R. D., and D. Cook, 2013: The role of vortex and environmental errors in genesis forecasts of Hurricanes Danielle and Karl (2010). *Mon. Wea. Rev.,* **141,** 232–251.

Wang, Z., M. T. Montgomery, and C. Fritz, 2012: A first look at the structure of the wave pouch during the 2009 PREDICT-GRIP dry runs of the Atlantic. *Mon. Wea. Rev.,* **140,** 1144–1163.

Weng, Y., and F. Zhang, 2012: Assimilating airborne Doppler radar observations with an ensemble Kalman filter for convection-permitting hurricane initialization and prediction: Katrina (2005). *Mon. Wea. Rev.,* **140,** 841–859.

Whitaker, J. S., and T. M. Hamill, 2002: Ensemble data assimilation without perturbed observations. *Mon. Wea. Rev.,* **130,** 1913–1924.

Zhang, F., and D. Tao, 2013: Effects of vertical wind shear on the predictability of tropical cyclones. *J. Atmos. Sci.,* **70,** 975–983.

——, C. Snyder, and J. Sun, 2004: Impacts of initial estimate and observation availability on convective-scale data assimilation with an ensemble Kalman filter. *Mon. Wea. Rev.,* **132,** 1238–1253.

——, Y. Weng, J. A. Sippel, Z. Meng, and C. H. Bishop, 2009: Cloud-resolving hurricane initialization and prediction through assimilation of Doppler radar observations with an ensemble Kalman filter. *Mon. Wea. Rev.,* **137,** 2105–2125.

——, J. F. G. Y. Weng, and F. D. Marks, 2011: Performance of convection-permitting hurricane initialization and prediction during 2008–2010 with ensemble data assimilation of inner-core airborne Doppler radar observations. *Geophys. Res. Lett.,* **38,** L15810, doi:10.1029/2011GL048469.